

Membrane Reserves and Hypotonic Cell Swelling

Nicolas Groulx¹, Francis Boudreault¹, Sergei N. Orlov^{1,2}, Ryszard Grygorczyk^{1,2}

¹Research Centre, Centre hospitalier de l'Université de Montréal–Hôtel-Dieu, 3850 Saint-Urbain, Montréal, Québec Canada H2W 1T7

²Department of Medicine, Université de Montréal, C.P. 6128 Succursale Centre Ville, Montréal, Québec H3C 3J7, Canada

Received: 29 September 2006/Revised: 7 November 2006

Abstract. To accommodate expanding volume (V) during hyposmotic swelling, animal cells change their shape and increase surface area (SA) by drawing extra membrane from surface and intracellular reserves. The relative contributions of these processes, sources and extent of membrane reserves are not well defined. In this study, the SA and V of single substrate-attached A549, 16HBE14o⁻, CHO and NIH 3T3 cells were evaluated by reconstructing cell three-dimensional topology based on conventional light microscopic images acquired simultaneously from two perpendicular directions. The size of SA reserves was determined by swelling cells in extreme 98% hypotonic (~6 mOsm) solution until membrane rupture; all cell types examined demonstrated surprisingly large membrane reserves and could increase their SA 3.6 ± 0.2 -fold and V 10.7 ± 1.5 -fold. Blocking exocytosis (by *N*-ethylmaleimide or 10°C) reduced SA and V increases of A549 cells to 1.7 ± 0.3 -fold and 4.4 ± 0.9 -fold, respectively. Interestingly, blocking exocytosis did not affect SA and V changes during moderate swelling in 50% hypotonicity. Thus, mammalian cells accommodate moderate (<2-fold) V increases mainly by shape changes and by drawing membrane from preexisting surface reserves, while significant endomembrane insertion is observed only during extreme swelling. Large membrane reserves may provide a simple mechanism to maintain membrane tension below the lytic level during various cellular processes or acute mechanical perturbations and may explain the difficulty in activating mechanogated channels in mammalian cells.

Key words: Cell volume — Membrane reserve — Membrane stretch — Three-dimensional cell imaging

Electronic Supplementary Material is available in the online version of this article at: <http://dx.doi.org/10.1007/s00232-006-0080-8>

Correspondence to: R. Grygorczyk; email: ryszard.grygorczyk@umontreal.ca

Introduction

Despite the lack of a rigid wall, animal cells are capable of controlling their shape, volume (V) and surface area (SA), responding to physical perturbations by triggering appropriate regulatory mechanisms. In particular, osmotic stress-induced V changes, which disrupt the optimal concentration of intracellular enzymes and metabolites, activate a cell-specific set of membrane transporters, leading to regulatory volume decrease (RVD) or increase (McManus, Churchwell & Strange, 1995; Strange, 2004). Because swellings may involve stretching of the surface membrane and increase lateral membrane tension, activation of mechanosensitive channels is often suggested as a possible cell V sensor and trigger of RVD (reviewed in Mongin & Orlov, 2001). The membrane lipid bilayer can expand ~3% in area before rupture (Nichol & Hutter, 1996; Hamill & Martinac, 2001) and, thus, offers very limited room for SA and V increase. However, irregularly shaped, substrate-adherent cells could utilize several other processes to accommodate expanding V, including shape changes and increased SA, by drawing extra membrane from intracellular reserves or from excess plasma membrane, i.e., SA reserves preexisting on the cell surface. This may smooth out surface irregularities, membrane folds and protrusions.

The size of membrane reserves reported in the literature varies considerably, depending on the cell type and measurement method: <1% was found in fibroblasts by pulling a membrane tether with optical tweezers (Raucher & Sheetz, 1999), up to ~70% was detected in lymphocytes from capacitance changes in whole-cell patch-clamp experiments (Ross, Garber & Cahalan, 1994), ~50% up to ~300% was reported in neurons by morphometry (Wan, Harris & Morris, 1995; Zhang & Bourque, 2003) and >500% was estimated in *Xenopus* oocytes (Zhang & Hamill, 2000) from electron microscopic images (reviewed in

Hamill & Martinac, 2001; Morris & Homann, 2001). SA reserves allow animal cells to buffer rapid fluctuations in membrane tension and to maintain it well below the lytic level. It is speculated, however, that local tension could reach sublytic levels, sufficient to activate mechanosensitive channels if the membrane is locally constrained by specialized, as yet not well-defined hypothetical structures (Hamill & Martinac, 2001; Morris & Homann, 2001). Localized changes of membrane tension could also regulate cell SA via tension-dependent exo-/endocytosis (Morris & Homann, 2001).

With a few exceptions, to our knowledge, it has not been systematically tested to what extent different animal cells increase their V and SA before significant surface membrane tension develops and membrane rupture occurs. How much of SA could be drawn from intracellular reserves or from excess surface membrane? Determining the contribution of these different processes to the SA increase during cell swelling may help to better understand how cells respond to physical stresses and the role of increased membrane tension in SA and V regulation.

In this study, we used an imaging technique developed recently in our laboratory, which allows reconstruction of cell three-dimensional (3D) topography, based on conventional light microscopic images acquired from two perpendicular directions (Boudreault & Grygorczyk, 2004b). Optically resolved cell SA and V could be calculated from a reconstructed 3D cell model. With this approach, we found that A549, 16HBE14o⁻, NIH 3T3 and Chinese hamster ovary (CHO) cells could increase their V > 10-fold and SA > 3.5-fold by drawing excess membrane from reserves. Although intracellular membrane reserves are larger than surface reserves, they do not play a significant role during modest (< 2-fold) cell swelling. Large membrane reserves in epithelial cells and fibroblasts indicate that in most physiological situations tension of the unconstrained lipid bilayer is unlikely to rise significantly, e.g., to levels required for activation of mechanogated channels. This would necessitate specialized structures to enable local membrane bilayer stress to rise significantly above that of the rest of the cell surface membrane.

Materials and Methods

CELLS

Human lung carcinoma A549 cells and murine NIH 3T3 fibroblasts were grown in Dulbecco's modified Eagle medium (DMEM) supplemented with 10% fetal bovine serum (FBS), 20 mM L-glutamine, 60 U/ml penicillin-G and 60 µg/ml streptomycin. Human bronchial epithelial 16HBE14o⁻ cells, a generous gift from Dr. D. Gruenert, were cultured in minimal essential medium (MEM), 10% FBS, 1% penicillin-streptomycin, 1% L-glutamine and 2.2 g/liter NaHCO₃, as described (Cozens et al., 1994). CHO cells were cultured in

α-MEM containing L-glutamine and complemented with 8% FBS, 1% penicillin-streptomycin. We also used CHO cells stably transfected with CFTR, which were cultured in the presence of 100 µM methotrexate. Because we found no differences in their V and SA responses, the data were pooled together. All constituents of the culture media were from Invitrogen (Burlington, ON, Canada). Cellular morphology was analyzed from cells plated at low density on 22 × 22 mm glass coverslips.

EVALUATION OF CELL V AND SA

To evaluate SA and V changes of substrate-attached cells, we used the upgraded version of a 3D imaging technique described in our previous work (Boudreault & Grygorczyk, 2004b). The following is a brief description of the improved method.

Top- and Side-View Images

The method involves 3D reconstruction of cell shape based on conventional light microscopic cell images acquired from two perpendicular directions. Cells grown on glass substrate were mounted in a custom-designed side-view chamber placed on the stage of a Nikon (Montreal, Canada) TE300 inverted microscope and continuously perfused with prewarmed saline (37°C, 1.3 ml/min) (Fig. 1). Vertical mounting of the coverslip permitted visualization of the lateral shape of the cell of interest close to the lower edge via a ×20 phase contrast objective. In addition, top-view images of the same cell were recorded via a second microscope objective (×10) attached to a phototube and mounted on a mechanical micromanipulator (MX 100; Newport Instruments, Mississauga, Canada) perpendicularly to the first objective (Fig. 1). Side- and top-view cell images were acquired simultaneously at 10- to 60-s intervals prior to hypotonic challenge and at 5- to 30-s intervals during the challenge, to closely follow rapid cell V changes. Images of the cell side-view profile and top view of the cell base were recorded for 100 ms with two independent miniature charge-coupled device cameras (MotiCam 350; Motic Instruments, Richmond, BC, Canada) and Motic software at 0.14-µm/pixel and 0.18-µm/pixel resolutions for side-view and top-view images, respectively. The images were saved on a hard disk and analyzed off-line.

Cell Surface Reconstruction and Visualization

The 3D topography of the cell surface was reconstructed by a dual-image surface reconstruction (DISUR) technique (Boudreault & Grygorczyk, 2004b). This technique generates a set of topographical curves of the cell surface from its digitized profile and base outline. Cell V, surface and height were calculated from such a reconstructed cell topographical model. All calculations were made entirely with Mat Lab (MathWorks, Natick, MA). To visualize the reconstructed cell model in 3D perspective, data obtained with the help of the DISUR technique were used to generate a 2D matrix containing approximate z coordinates of points on the membrane surface. The 3D perspective of the model cell was then plotted with Mat Lab or ORIGIN (Microcal Software, Northampton, MA).

SOLUTIONS AND CHEMICALS

Physiological saline solution contained (in mM) 140 NaCl, 5 KCl, 1 MgCl₂, 1 CaCl₂, 10 glucose and 10 4-(2-hydroxyethyl)-1-piperazineethanesulfonic acid (HEPES) (pH 7.4), adjusted with NaOH. We prepared 50% hypotonic media by reducing NaCl concentration while keeping divalent cation concentration constant. The 98% hypotonic solution (~6 mOsm) contained only 1 mM MgCl₂ and 1 mM CaCl₂. Because hypotonic solutions were prepared by reducing

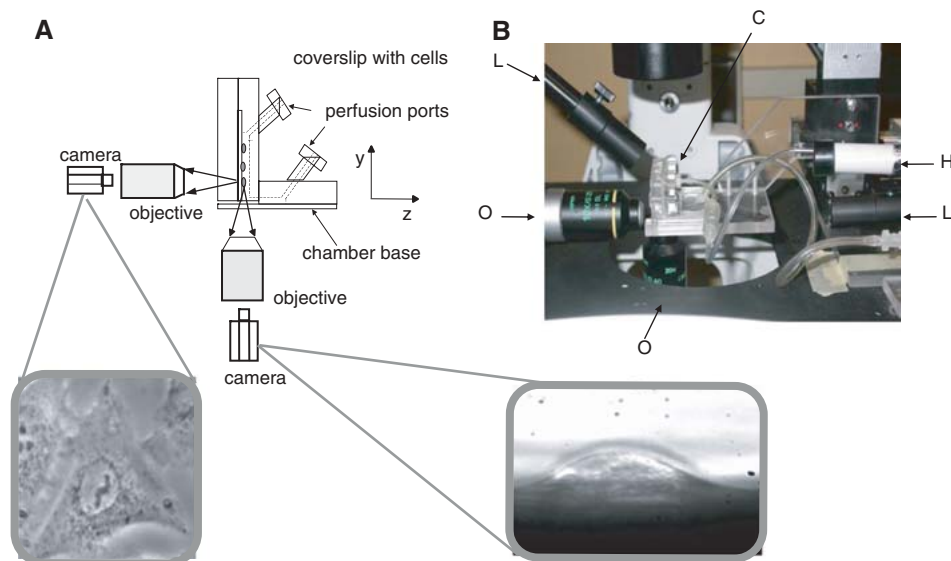


Fig. 1. Flow chamber and dual-image microscopy setup. (A) Functional diagram of flow chamber (adapted from Boudreault & Grygorczyk, 2004b). The acrylic chamber permits simultaneous microscopic observation of the cell side-view and top-view profiles. A standard 22×22 mm coverslip with adherent cells is positioned vertically along the inner chamber wall. In this orientation, the lower edge is facing the vertically oriented microscope phase contrast objective (objective 1, Nikon Ph 1 DL, $\times 20$). The second objective (objective 2, Nikon Ph DL, $\times 10$) is attached to the phototube and mounted horizontally on the mechanical micromanipulator (Newport Instruments). When both objectives are aligned in one plane, the same cell can be viewed from two perpendicular directions. The nominal depth of the chamber is approximately 0.5 mm and the total inner volume, $\sim 200 \mu\text{l}$. Images of a substrate-adherent cell profile and top view are recorded simultaneously with the two independent digital Moticam 350 cameras. The chamber cavity is perfused with a warm solution (37°C). The orientation of the Cartesian coordinate system shown here is used in off-line image analysis. (B) Photograph of the chamber mounted on the stage of an inverted Nikon TE-300 microscope. The two perpendicularly oriented objectives are also visible. C, chamber; H, inline solution heater; L, fiber-optic light source; O, microscopy objective.

salt concentration, both osmolarity and ionic strength were reduced. All reagents, including *N*-ethylmaleimide (NEM), were from Sigma-Aldrich (Oakville, Canada). For experiments at low temperatures, a custom-made in-line cooler was used. It consisted of a small container filled with ice-saturated water, which allowed the solution temperature to be reduced to 10°C at the inlet of the experimental chamber. To block exocytosis, A549 cells were pre-treated with 1 mM NEM for 15 min at room temperature, and cell swelling was examined at 37°C after washing.

Results

RESTING CELL SA AND V

Sample images of A549, 16HBE14o⁻, NIH 3T3 and CHO cell side profiles, observed under resting conditions in isotonic solution, and the perspective view of their reconstructed 3D models are shown in Figure 2A and B, respectively. Epithelial A549 and 16HBE14o⁻ cells tended to be more flat than CHO and NIH 3T3 fibroblasts, which were generally more rounded, especially in a group of cells. Figure 2C summarizes the average initial SA (SA_0 , in μm^2) and initial cell V (V_0 , in pL, 1 pL = $1,000 \mu\text{m}^3$) for the four cell types studied. All cell types had comparable SA_0 and V_0 , but these parameters varied significantly between individual cells; the SA_0 values were in the range $1,000$ – $3,500 \mu\text{m}^2$, while V_0 values were in the

range 2 – 7 pL. The SA_0 to V_0 ratios were significantly higher than those calculated for spherical cells of similar V, indicating that resting cells have significant room for V increase by changing their shape without SA augmentation (Table 1).

CELLS HAVE LARGE MEMBRANE RESERVES

The two principal strategies to accommodate cell V expansion are changes in cell shape and/or increased SA, utilizing membrane from reserves. To evaluate the size of the membrane reserves, the cells were swollen in extreme 98% hypotonic solution, and their SA and V were monitored in a dual-view chamber until cell membrane rupture. At the top of Figure 3A are examples of A549 cell side-view images recorded during such swelling experiments with their reconstructed 3D models shown below. The time course of SA and V changes for six individual cells with an average from 10 experiments is shown on the graphs below. After the onset of 98% hypotonic shock (at $t = 0$), the cells swelled rapidly at the rate of $> 100\%$ V increase per minute. During this initial swelling phase, the cells underwent significant shape changes (rounding up); and at ~ 7.5 -fold V increase ($t \approx 3.5$ min), they started to partially detach from the substrate, as seen by significant outline changes of the

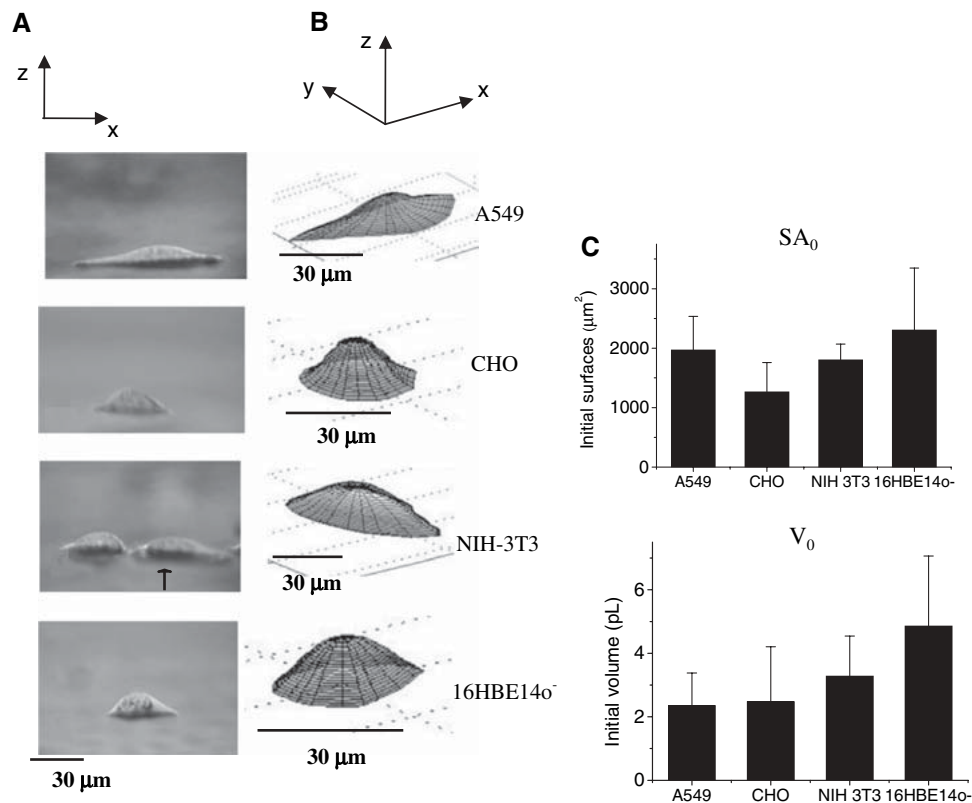


Fig. 2. SA and V of resting cells. (A) Examples of light microscopic side-view images of resting, substrate-attached A549, CHO, NIH 3T3 and 16HBE140⁻ cells. The corresponding perspective view of 3D cell models, reconstructed by the DISUR technique (as described in Materials and Methods), is shown in B. Of the two NIH 3T3 cells seen in A, the *arrow* indicates the cell whose reconstructed model is shown in B. (C) Average (\pm sd) SA₀ (in μm^2) and V₀ (in pL, 1 pL = 1,000 μm^3) of resting cells for the four different cell types measured under isotonic solution. The data are from 8–10 measurements.

Table 1. Initial rates (\pm sd) of cell V expansion during 98% hypotonic shock, expressed as x-fold initial V increase/min, and corresponding S₀/V₀ ratios

	Initial rate (fold/min)	S ₀ /V ₀ (μm^{-1})
A549 (<i>n</i> = 4)	1.70 \pm 0.13	0.59 \pm 0.14
A549 + trypsinization (<i>n</i> = 7)	0.98 \pm 0.07	0.35 \pm 0.27
16HBE140 ⁻ (<i>n</i> = 10)	1.54 \pm 0.12	0.47 \pm 0.47
NIH 3T3 (<i>n</i> = 9)	1.66 \pm 0.03	0.55 \pm 0.21
CHO (<i>n</i> = 9)	2.01 \pm 0.03	0.51 \pm 0.28

Rates refer to the first 2–3 min of cell swelling; *n*, number of experiments.

cell base in the top-view images. After reaching a near spherical shape, the highest V/SA ratio, the cells continued to swell until the membrane ruptured, typically between \sim 7 and \sim 15 min. Membrane rupture was determined on the basis of several criteria: (1) a subtle but sudden decrease in cell V, occasionally associated with a partial release of intracellular content; (2) a sudden change in nucleus image contrast; and (3) trypan blue uptake, observed only after

events (1) and (2), consistent with membrane rupture at this point.

The maximal A549 cell SA increase at the time of cell burst was 3.8 ± 1 -fold (*n* = 10) and, for V, 12.9 ± 1.7 -fold (*n* = 10). Similar results were obtained with the three other cell types examined in this study: 16HBE140⁻, NIH 3T3 and CHO fibroblasts (Fig. 3B–D, respectively), although some differences in the swelling time course as well as initial and final rates of swelling could be noticed. Figure 4 summarizes the results of these experiments for the four cell lines and shows average values (\pm standard deviation [SD]) of the maximal cell SA and V increase at the time of cell burst (Fig. 4A and B, respectively). Total cell SA reserves were very large; the average for all cell types was 3.6 ± 0.2 -fold of SA₀ (*n* = 38). All cell types also presented similar maximal V increases of 10.7 ± 3.2 -fold (*n* = 38). Figure 4C reveals that A549 and 16HBE140⁻ cells could sustain such shock typically for approximately 10 min, while the two fibroid cell lines, NIH 3T3 and CHO, showed approximately a twofold shorter time of burst. Because the final V of all cells at burst was similar, this is consistent with the higher average swelling rate of fibroblasts compared to epithelial A549 and

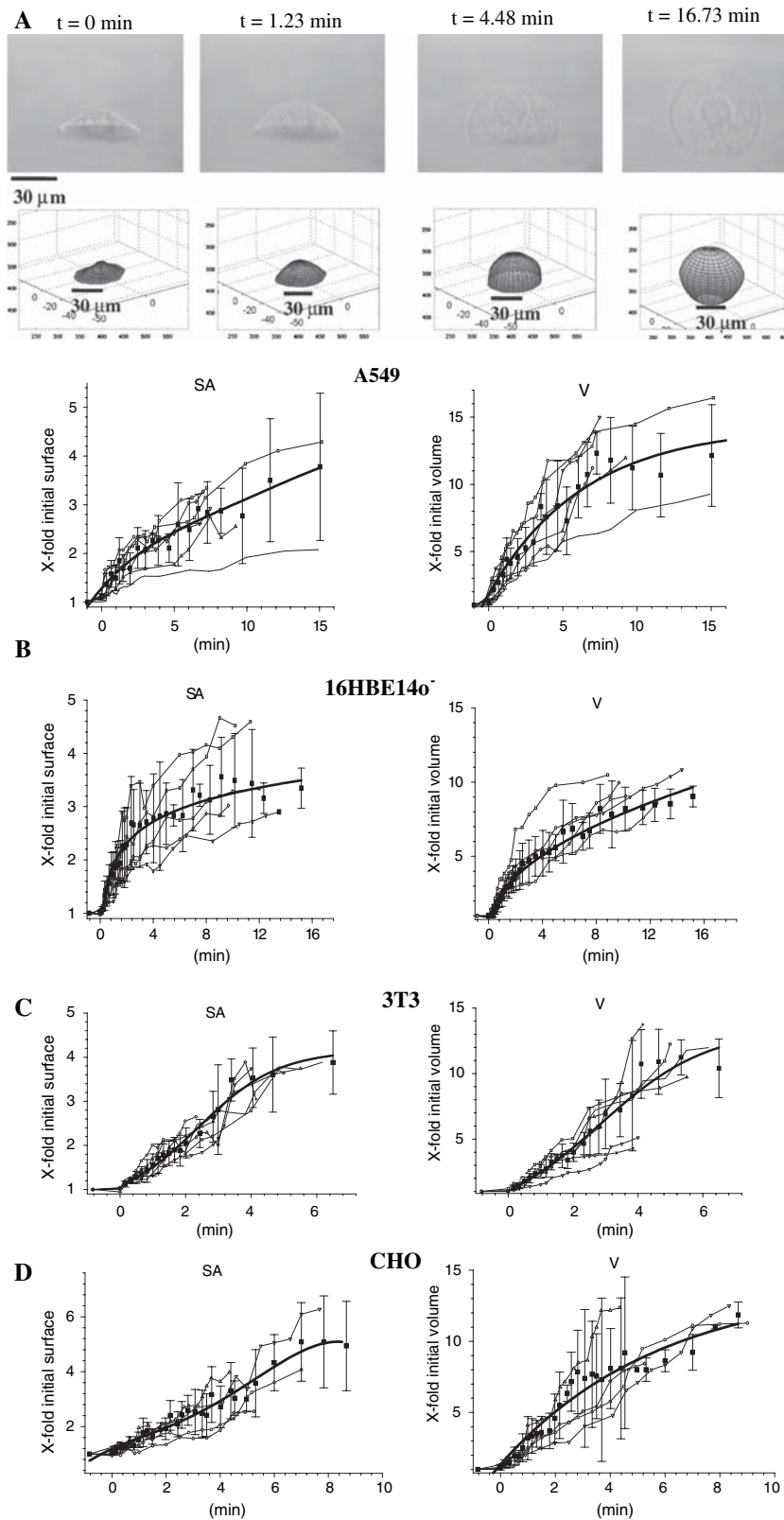


Fig. 3. Time course of cell SA and V changes during swelling in 98% hypotonic solution. (A) A sequence of side-profile images and 3D cell reconstructions showing changes of A549 cell shape and size during swelling in 98% hypotonic solution at different time points after the onset of hypotonic shock. Graphs present the time course of SA (*left*) and V (*right*) changes. *Small symbols and thin lines* represent data from individual single-cell experiments. For clarity, only six individual experiments are illustrated. *Thick symbols* represent the average data (\pm SD) from 10 experiments, and *solid lines* represent best fit to the average data (exponential or polynomial functions). (B–D) Similar data for human bronchial epithelial cells 16HBE140⁻, mouse NIH 3T3 fibroblasts and CHO cells, respectively. Four to 10 representative traces from individual single-cell experiments are depicted for each cell type. The cells were perfused with a warm (37°C) isotonic solution (~300 mOsm), and at time 0, the perfusate was changed to 98% hypotonic (~6 mOsm) solution. Side-view and top-view cell images were recorded until cell burst, which is the last point for each thin-line trace. Cell SA and V were calculated off-line by the DISUR approach (see Materials and Methods).

16HBE140⁻ cells. As can be seen from the time course of V changes in Figure 3, the initial swelling rates of all cell lines were comparable, between 1.5- and 2-fold/min (Table 1). However, they declined

significantly during the course of swelling for epithelial cells, while fibroblasts showed a more linear swelling time course and higher final swelling rates before cell burst (Fig. 3). The swelling rate of A549

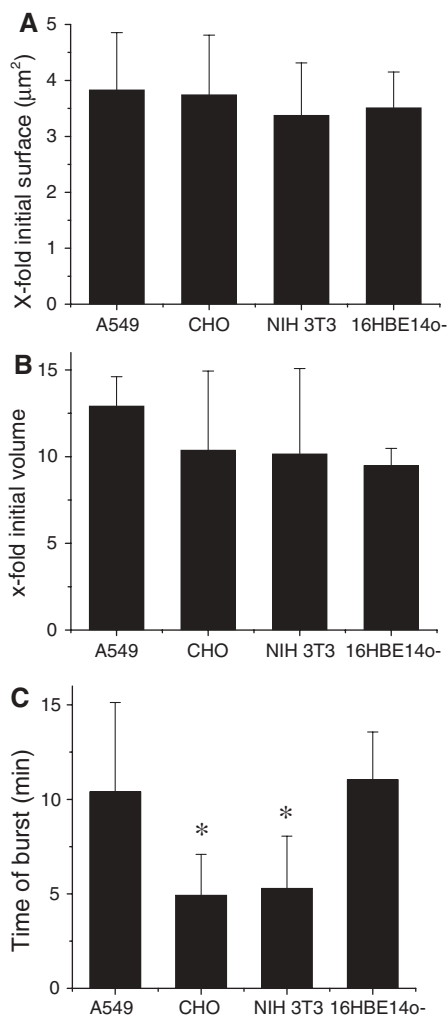


Fig. 4. SA and V of maximally swollen cells at the time of burst in 98% hypotonicity. Maximal cell SA (SA_{max}) and volume (V_{max}) recorded at the time of cell burst in 98% hypotonic solution are shown in *A* and *B*, respectively. Average values \pm SD are presented, $n = 10$ experiments for each cell type. (*C*) Average time (\pm SD) between the onset of 98% hypotonic shock and cell burst, $n = 10$. Note the shorter burst time for the two fibroblast NIH 3T3 and CHO cell lines compared to A549 and 16HBE14o⁻ epithelial cells; the differences were statistically significant, as determined by Student-Newman-Keuls test, * $P < 0.05$.

cells changed significantly after trypsin treatment (*see below*).

CONTRIBUTION OF ENDOMEMBRANES TO SA RESERVES DURING 98% HYPOTONIC SWELLING

During V expansion, the cells could draw extra membrane from surface structures, such as membrane folds and protrusions, and from the intracellular pool by exocytosis. To evaluate the relative contributions of the intracellular and surface pool of membrane reserves, A549 cells were swollen in 98% hypotonic solution after blocking exocytosis.

Two approaches were taken to block exocytosis, low temperature (Renstrom et al., 1996) and treatment with NEM, a sulfhydryl-modifying agent which inhibits vesicular exocytosis by acting on NEM-sensitive proteins of the soluble NEM-sensitive factor attachment protein (SNAP) receptor (SNARE) complex (Jackson & Modern, 1990). Figure 5A shows that at 10°C A549 cells swelled at a significantly slower rate of 6–10%/min, compared to ~100–200%/min at 37°C. The cells ruptured after 50–60 min. At the time of burst, the maximal increases of cell SA and V were 1.9 ± 0.4 -fold and 4.6 ± 0.4 -fold, respectively (Fig. 5C). These values were significantly reduced compared to those observed at 37°C. When exocytosis was blocked by NEM treatment and the cells were swollen at 37°C, 8 of 10 cells examined showed only limited swelling but several membrane blebs developed. During the experiment, these blebs often fused into a single large bleb, which increased in size until rupture. Assuming that NEM treatment completely blocked exocytosis, bleb formation was only possible from preexisting surface membrane. Thus, membrane bleb size at the time of its rupture would indicate the amount of membrane available on the cell surface. We found that the maximal SA increase of the cell plus the bleb was 1.6 ± 0.3 -fold, while the corresponding V increase was 4.2 ± 1.5 -fold at the time of burst (Fig. 5B, C). This was very similar to the cell SA and V enlargement observed at 10°C. The 2 of 10 cells which did not develop visible blebs during swelling showed smaller (<3-fold) V increases when ruptured, likely because larger bleb formation was somehow restricted by the rigid cell membrane skeleton; therefore, these two experiments were excluded from further analysis. The above experiments revealed that during extreme 98% hypotonic swelling approximately two-thirds of the total cell SA increase was due to membrane recruitment from the intracellular pool via exocytosis, while the remaining SA augmentation could be attributed to unfolding and smoothing-out of excess surface membrane.

CONTRIBUTION OF ENDOMEMBRANE EXOCYTOSIS TO SA CHANGES DURING 50% HYPOTONIC SWELLING

We then examined the relative contributions of the two processes, i.e., exocytosis and membrane unfolding, to SA and V changes during moderate cell swelling in 50% hypotonicity. Figure 6A reports the time course of A549 cell SA and V increases under control conditions at 37°C. The cells reached peak V at approximately 2 min, followed by RVD, which was completed within the next ~15 min. The maximal V expansion was $\sim 82 \pm 12\%$, while SA increased by $\sim 29 \pm 14\%$, similar to that observed in our previous studies (Boudreault & Grygorczyk, 2004a, 2004b).

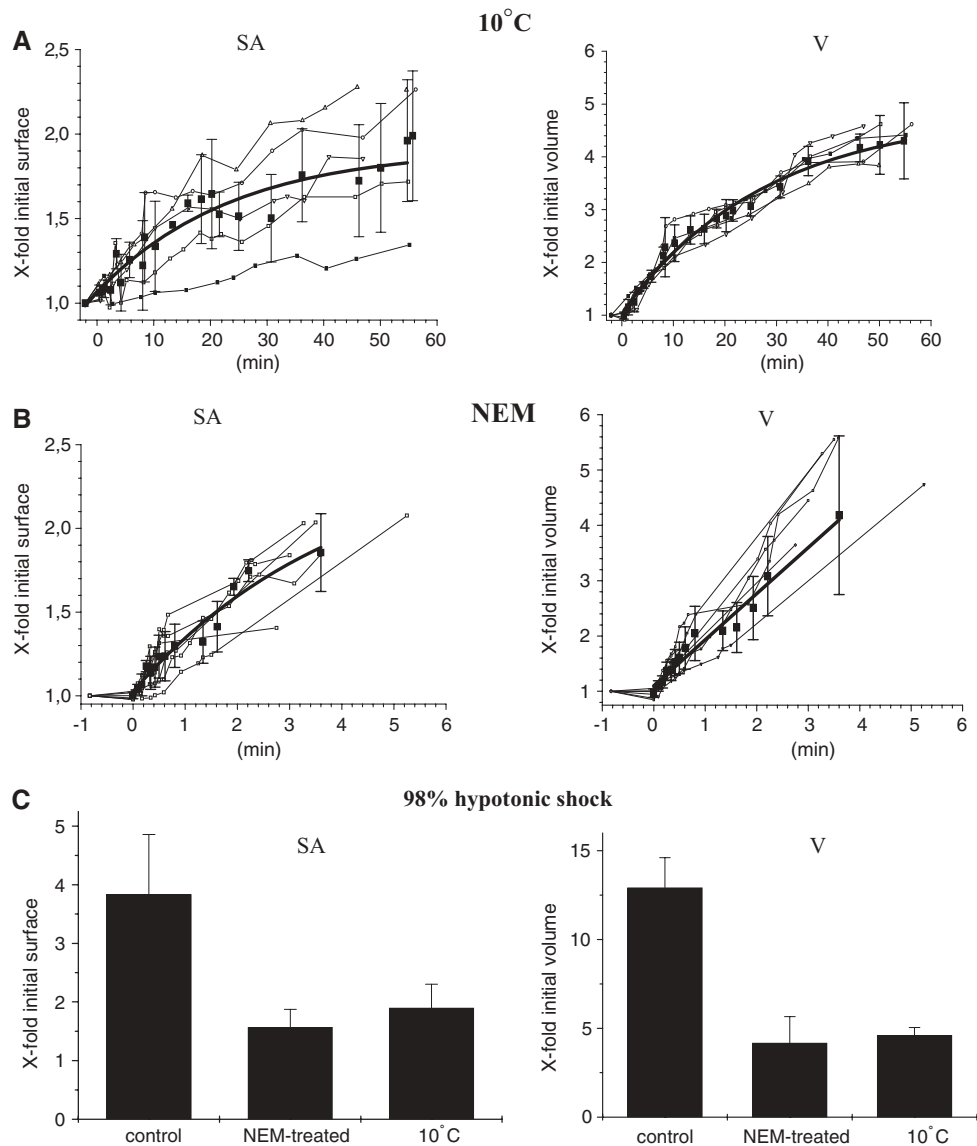


Fig. 5. Time course of A549 cell swelling in 98% hypotonicity after blocking exocytosis. (A) Time course of cell SA and V increases during swelling in 98% hypotonicity at 10°C. (B) Time course of cell SA and V increases during swelling in 98% hypotonicity after treatment with NEM. With NEM-treated cells, swelling resulted in membrane bleb formation, which made it difficult to evaluate total cell SA and V. Total SA and V were calculated in such situations as SA or V of a cell plus bleb. These evaluations, however, were possible only with cells having a single bleb or after several smaller blebs fused together into a large single bleb later during the experiment. Therefore, for some experiments, no data points are shown for the period when several membrane blebs were present. *Small symbols and thin lines* represent data from individual single-cell experiments. For clarity, only four to five individual experiments are illustrated. *Thick symbols* represent average data (\pm SD) from 8 to 10 experiments, and *solid lines* represent exponential fit to the average data. (C) Average maximal SA and V increase in 98% hypotonic solution. Blocking exocytosis by low temperature (10°C) or NEM treatment significantly reduced maximal SA and V increases.

When exocytosis was blocked by reducing the temperature to 10°C, the cells swelled at a decreased rate, reaching a peak V of 76% at 4–6 min. RVD was abolished at this temperature (Fig. 6B). When the cells were pretreated with NEM and swelling was examined at 37°C (Fig. 6C), the rate of swelling and the average peak V (\sim 1.7-fold) were not significantly affected. The cell SA increase was also comparable to that of untreated cells (Fig. 7). Interestingly, NEM treatment completely impaired the RVD; after a peak

at 2–3 min, cell V dropped only slightly from 168% at the peak to 150%, and remained unchanged during the remaining 15 min of the experiment. The SA and V changes induced by 50% hypotonic shock under different experimental conditions are summarized in Figure 7. These experiments demonstrate that during moderate (\leq 2-fold) swelling cells increase their SA by \sim 30%, mainly by unfolding the surface membrane, while the contribution of the intracellular membrane pool is negligible under these conditions.

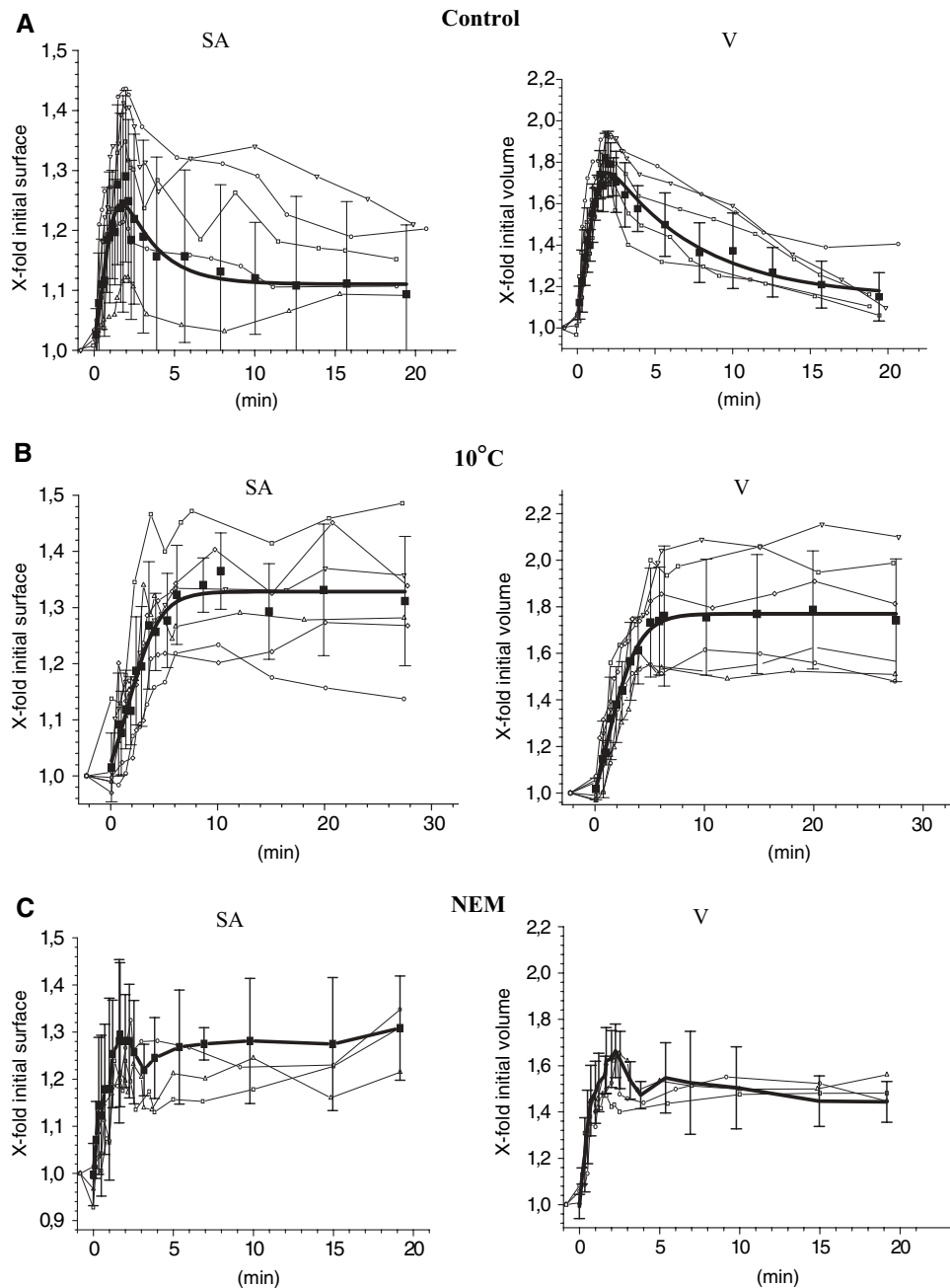


Fig. 6. Time course of A549 swelling in 50% hypotonicity. (A) Time course of A549 cell SA and V increases during swelling in 50% hypotonicity at 37°C. (B) Swelling of A549 cells at 10°C. Note the significantly slower kinetics of cell swelling and lack of RVD, although maximal V and SA were similar to those observed at 37°C. (C) NEM-treated cell swelling at 37°C is similar to that of control, untreated cells but RVD is absent. *Small symbols and thin lines* represent data from individual single-cell experiments. For clarity, only four to five individual experiments are shown. *Thick symbols* represent the average data (\pm SD) from 8 to 10 experiments, and *solid lines* represent a fit to the average data.

ROLE OF SUBSTRATE ATTACHMENT IN CELL SWELLING

The initial rate and time course of swelling varied significantly between individual cells, and this may have been due in part to differences in cell substrate attachment and, thus, in initial cell shape and SA. Substrate attachment may have influenced the rate of swelling in several ways, e.g., by restricting water flux

across the cell base and, hypothetically, providing greater mechanical support for the cell membrane to resist V expansion. To determine if substrate attachment influenced the initial rate, time course and extent of hypotonic swelling, A549 cells were mounted in a dual-view perfusion chamber and briefly exposed to trypsin (0.05%, 3–5 min, 37°C) in a Ca^{2+} -free solution. When the cells rounded up and

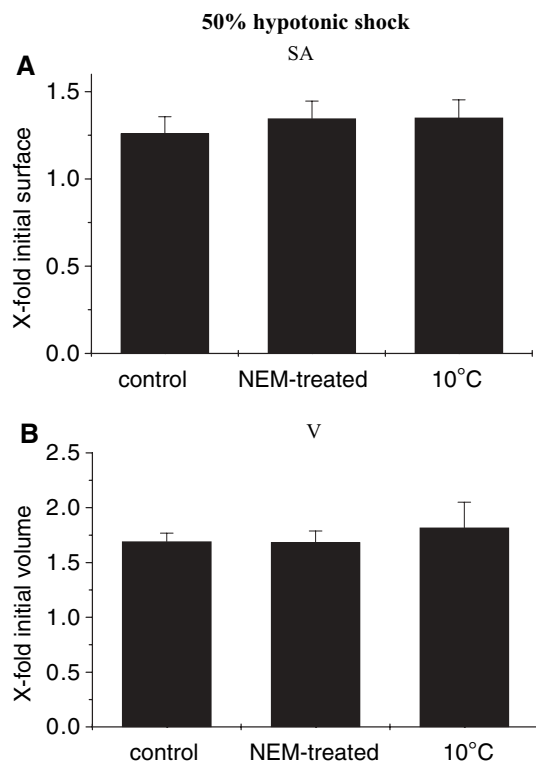


Fig. 7. Effect of blocking exocytosis on SA and V increase during 50% hypotonic swelling. Graphs show the average of maximal SA (A) and V (B) increase of A549 cells in 50% hypotonic solution. Blocking exocytosis by low temperature (10°C) or NEM treatment had no effect on SA or V changes. This contrasts with the data for 98% hypotonic swelling shown in Figure 5C. For each experimental condition, $n = 10$; all SA and V changes were statistically not significant (Student-Newman-Keuls test, $P < 0.05$).

almost completely detached from the substrate, except for a small adherence area that still kept them in place (Fig. 8), trypsin was washed away. We found that during trypsinization cell V remained constant but cell SA was reduced by $25 \pm 12\%$ ($n = 6$; Fig. 8A, B). A similar decrease was observed for the portion of cell SA that was directly facing the extracellular medium ($26 \pm 10\%$). This confirms that resting, substrate-attached cells have a substantially higher SA/V ratio compared to rounded, trypsinized cells and, thus, have a potential to significantly increase V by simple shape changes. Subsequent exposure to 98% hypotonic solution resulted in rapid swelling, but the initial rate of swelling was reduced compared to substrate-attached cells (0.98- vs. 1.7-fold/min), in exact proportion to the decreased SA/V ratio (Table 1). The time course of swelling also showed less variability between individual trypsinized cells. The cell membrane ruptured at 9.2 ± 2.4 -fold initial V, i.e., similar to that seen with nontrypsinized cells. These experiments indicate that substrate attachment and cell shape do not affect the extent of cell swelling and the size of available

membrane reserves but may influence the time course and the initial rate of swelling, likely due to different SA/V ratios and associated differences in water fluxes.

Discussion

In this study, we measured SA and V of substrate-attached cells using a dual-image 3D cell reconstruction technique developed in our laboratory. We determined the upper limits of the SA and V increase by swelling cells in extreme ~ 6 mOsm hypotonic solution and found that all four cell types tested, A549, 16HBE14o⁻, NIH 3T3 and CHO, have a surprisingly large capacity to augment their SA more than ~ 3.5 -fold and V more than ~ 10 -fold. A large part of the SA increase in A549 cells was due to exocytotic insertion of endomembranes. Interestingly, this mechanism made a negligible contribution to the SA increment during modest (≤ 2 -fold) cell swelling.

SOURCES OF CELL SA AND THEIR CONTRIBUTION TO V EXPANSION

To accommodate V expansion, cells utilize two principal strategies: shape changes and SA elevation. The increase of SA could involve (1) drawing extra membrane from cell surface reserves by unfolding and smoothing out excess surface membrane, (2) exocytotic insertion of endomembranes and (3) lipid bilayer stretching (Fig. 9). Based on our experimental data with A549 epithelial cells, we could estimate the relative contributions of these processes to SA and V changes during extreme (98% hypotonic) and moderate (50% hypotonic) swelling. During extreme swelling, assuming that the lipid bilayer of maximally swollen (≥ 10 -fold) cells is stretched to its limit ($\sim 3\%$ area expansion) at the time of plasma membrane rupture, this would roughly correspond to 11% extra SA relative to the SA_0 of a resting cell. The contributions of surface and intracellular reserves were estimated from experiments in which exocytosis was blocked by low temperature (10°C) or NEM treatment. NEM, by thiol alkylation of cysteine residues, has a broad spectrum of cellular effects, altering the activity of enzymes, receptors, ion channels, transporters and transcription factors (Gilbert, 1990). It is also known to effectively block exocytosis via its action on SNARE, a set of conserved proteins involved in several steps of exocytosis, including vesicle transport, membrane docking and fusion. The two approaches of blocking exocytosis produced very similar results: at 10°C, the maximal SA increase was reduced from 3.8 ± 1.0 -fold ($\Delta SA \approx 280\%$) to 1.9 ± 0.4 -fold ($\Delta SA \approx 90\%$) and, in experiments at 37°C after NEM treatment, it decreased to

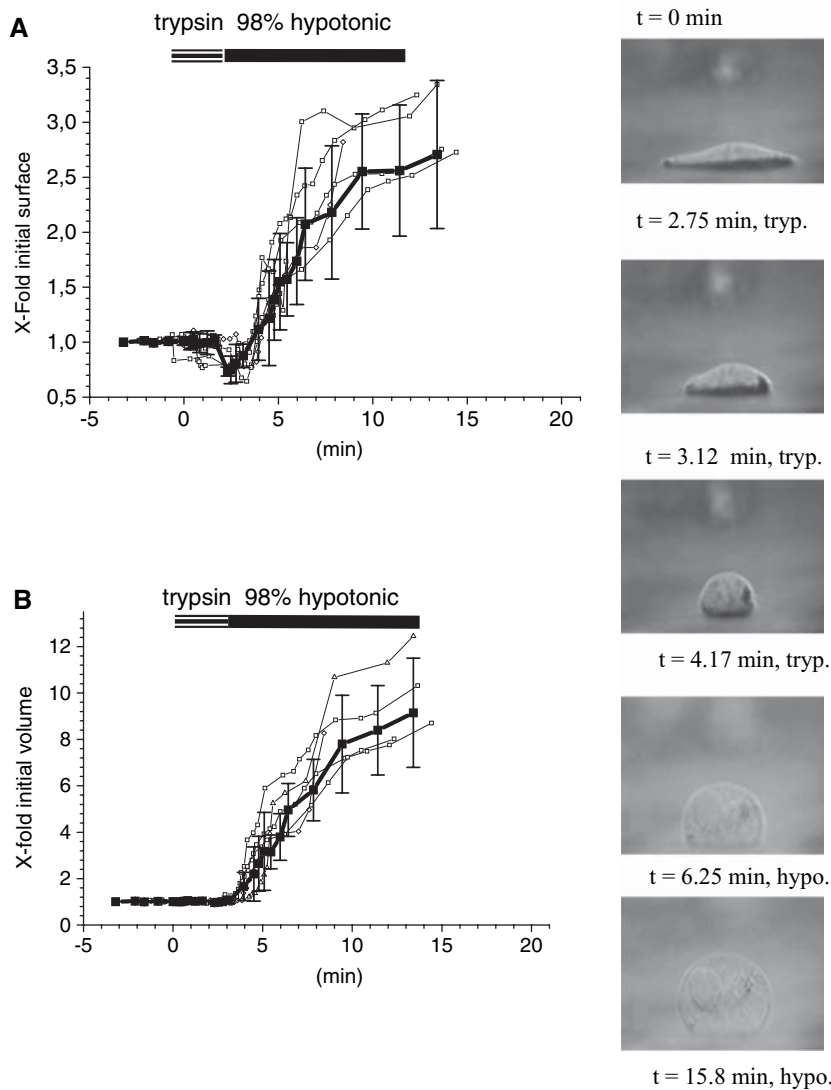


Fig. 8. Substrate attachment influences cell SA and the kinetics of hypotonic swelling. Time course of cell SA (*A*) and V (*B*) changes during trypsinization and subsequent swelling in 98% hypotonicity. Note the significant drop of SA and invariable V of trypsinized cells at $t = 4$ min. The *right column* shows a sequence of A549 cell side-profile images, which illustrate cell shape changes during trypsinization in isotonic solution at 37°C , frames at $t = 0-4$ min. This was followed by hypotonic swelling starting at ~ 4 min, frames 6.25 and 15.8 min. See video clip in the supplemental material.

1.6 ± 0.3 -fold ($\Delta\text{SA} \approx 60\%$) (Fig. 5C). Thus, on average, after blocking exocytosis, A549 cells were still capable of increasing their SA during extreme hypotonic swelling by approximately 75%, likely by utilizing membrane reserves preexisting on the cell surface. From these experiments, we could also conclude that the remaining approximately 200% of the SA increment was due to endomembrane exocytosis. Estimates of the relative contribution of different SA sources are summarized in Figure 9A, while Figure 9B shows the estimated contributions of these processes to the V increase. The contributions of shape changes were evaluated on the basis of the SA_0 of resting cells, illustrated in Figure 2, by calculating

the V of a spherical cell with the same SA. All other calculations were made for such a spherical cell by taking into account the SA increase due to endomembrane exocytosis, the use of surface reserves and lipid bilayer stretch. Thus, the largest $\sim 200\%$ contribution to the SA increment came from endomembrane exocytosis, corresponding to a $>600\%$ V enhancement. These were the upper limits that the processes could contribute, and they were determined by swelling cells under extreme 98% hypotonic conditions. In contrast, during moderate, e.g. ~ 2 -fold, swelling in 50% hypotonicity, we found that most of the A549 cell SA increase could be attributed to unfolding or smoothing out of existing surface

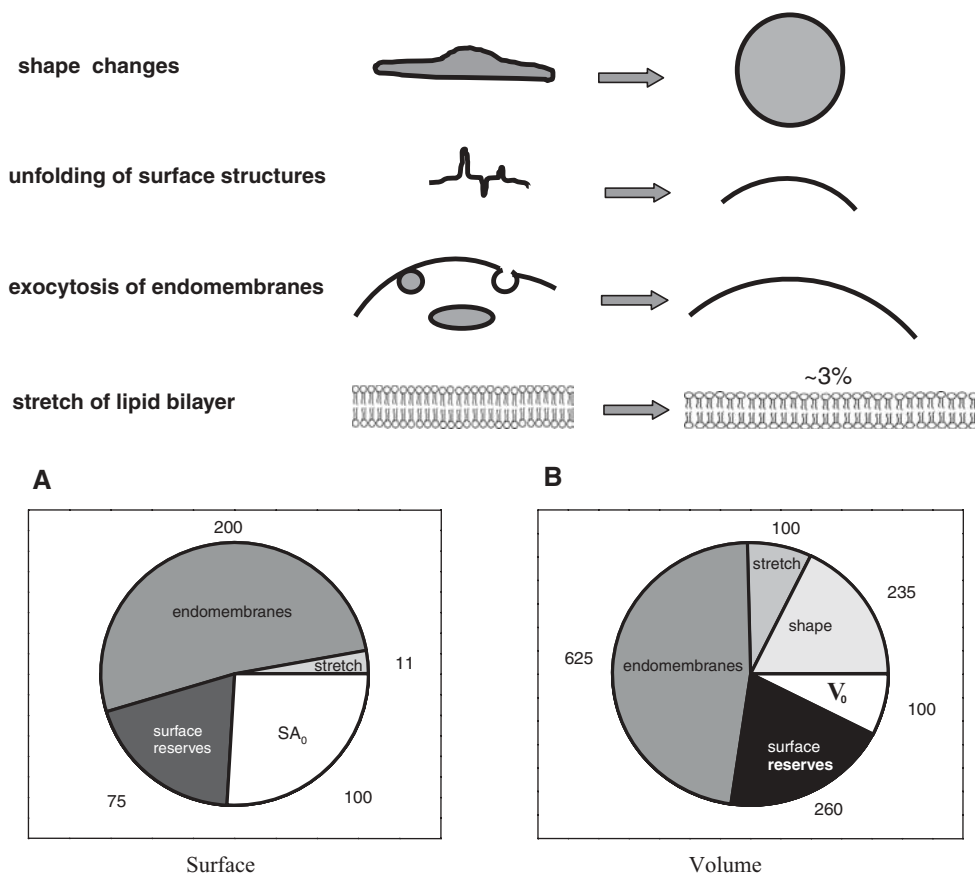


Fig. 9. Relative contribution of cell shape changes and SA reserves to hypotonic V expansion of A549 cells. Shown are four different processes that may contribute to V accommodation during hypotonic swelling. Pie graphs *A* and *B*, respectively, illustrate the relative contribution of these processes to SA and V increases during extreme swelling of A549 cells. SA₀ and V₀ represent surface area and volume of resting cell.

membrane, while exocytosis of endomembranes made a negligible contribution that was below the detection limit in our experiments ($\leq 5\%$) (Fig. 7). This was consistent with a similar observation on, e.g., astrocytes and hepatocytes, which also did not recruit additional membrane during moderate swelling, and no changes in electrical membrane capacitance were detected (Graf et al., 1995; Olson & Li, 1997). Lymphocytes could also swell at fixed capacitance up to twofold; beyond that, swelling recruits new membrane (Ross et al., 1994). Thus, cells use different pools of SA reserves, depending on the extent of V changes. Moderate V expansions are accommodated by shape alterations and the use of surface reserves, whereas endomembrane recruitment seems to predominate during extreme (>2 -fold) swelling. It is interesting to note that during swelling in 50% hypotonicity less than half of the total ($\sim 75\%$) available pool of cell surface reserves was used by A549 cells.

The large intracellular and surface membrane reserves found in our study contrast with a number of earlier reports. While it was recognized that some cell types (e.g., oocytes, macrophages and mast cells)

have large, excess surface membrane, this was not anticipated for other types (e.g., fibroblasts and epithelial cells) that respond to frequent changes of passive stretch or osmotic swelling (Hamill & Martinac, 2001). Previous studies indicated much smaller SA reserves: e.g., fibroblasts were reported to have a small bilayer reservoir of 0.3–1% of the total SA, as measured by pulling a bilayer tether (Raucher & Sheetz, 1999). The difference could be attributed to the fact that tether measurements relied on the assumption that membrane tension was continuous over the entire plasma membrane, which may not be fully the case, especially for adherent cells, where local perturbation (pulling the tether) could be spatially restricted (Morris & Homann, 2001). In contrast, in our experiments, we studied the effects of osmotic pressure acting on the entire plasma membrane.

It should also be noted that our SA reserve estimates were only qualitative, based on several assumptions and subject to several limitations. For example, the contribution of surface reserves might be underestimated because the maneuvers that we used to block exocytosis, low temperature and NEM

treatment, may also, at least partially, impair the cell's ability to draw membrane from surface reserves. This would also result in an overestimation of endomembrane contribution in our experiments. Indeed, NEM is known to cause an immediate cessation of all motile activities and simultaneous stabilization of the cell ultrastructure (Karlsson & Lindberg, 1985). The cell shape and SA changes that we observed in NEM-treated cells during hypotonic shock are unlikely to be due to residual membrane trafficking or motile activity but exclusively result from osmotic pressure acting on cell membrane and membrane-anchored cytoskeletal elements. We also observed membrane bleb development during swelling of NEM-treated cells, similar to that observed, e.g., during hypoxic and toxic injury to cells (Jewell et al., 1982). We assume that in the absence of exocytosis in NEM-treated cells the size of membrane blebs corresponds to membrane reserves preexisting on the cell surface. The mechanism of bleb formation is not fully understood, but there is a notion that it results from cytoskeletal disruption and disturbance in membrane-cytoskeleton connections. This may occur during metabolic poisoning because cellular microfilaments and microtubules are in a dynamic state of continuous formation and disassembly, processes that are highly energy-dependent (Lemasters et al., 1987). Furthermore, NEM was reported to induce membrane blebbing in other cell types, by weakening cytoskeleton linkage to membrane proteins. In platelets, the connection between the cytoskeleton and the membrane adhesion glycoprotein receptor GPIb involves filamin A (FLNa, previously called actin-binding protein APB-280), a dimeric actin cross-linking and scaffold protein with numerous intracellular binding partners (Nakamura et al., 2006). GPIb-FLNa interactions can be dissociated by thiol alkylation with NEM. A similar mechanism, i.e., disruption of membrane-cytoskeleton interactions in NEM-treated cells, could be responsible for the bleb formation observed in our study.

Our assumption that the lipid bilayer of entire cells is maximally stretched (by ~3%) at the time of membrane rupture is consistent with a membrane bilayer behaving as a fluid. This might be an overestimation, however, if the tension is not distributed uniformly and local tension gradients exist. Furthermore, we measured cell SA as resolved by light microscopy; thus, submicroscopic membrane structures, such as microvilli, membrane folds and other irregularities, could not be detected, and we considered them as a reservoir of cell SA. Therefore, our SA estimates may differ from those measured in whole-cell patch-clamp experiments as cell membrane electrical capacitance. Finally, we observed large variability of SA and V between individual cells, which were chosen randomly for our experiments. Such variability is expected as SA and V are altered

during many cellular processes, including the cell cycle. For example, during mitosis, cells need to double their SA; therefore, those with two clearly visible nuclei were rejected from our analysis.

ROLE OF SUBSTRATE ATTACHMENT IN CELL SWELLING

Our experiments disclosed that after trypsinization of A549 cells the total SA and its fraction directly facing the extracellular medium were significantly reduced. This could explain the observed decrease of the initial swelling rate of such cells by diminishing osmotic water flux. Indeed, the initial swelling rate correlated well with the initial SA_0/V_0 ratios of trypsinized *vs.* nontrypsinized A549 cells (Table 1). Similar correlations could be noticed for nontrypsinized remaining cell types, with the exception of CHO cells. An additional factor(s) affecting the swelling rate, not investigated in the present study, could involve different membrane water permeabilities and differences in membrane mechanical resistance to V expansion. In the context of the tensegrity model, cellular structure is mechanically stabilized by a prestressed framework composed of molecular struts, ropes and cables and is influenced by membrane-cytoskeleton interactions, extracellular matrix and substrate attachment (Ingber, 2003). In substrate-attached cells, SA varied during swelling, especially in 98% hypotonic solution, when the cells undergo significant shape changes and partially detach from the substrate. Therefore, differences in initial cell shape and extent of substrate attachment may have contributed to the large variability of the swelling time course observed between individual cells. Consistent with this view, trypsinized A549 cells of near-spherical shape showed a more uniform swelling time course similar to fibroblasts, which were less firmly attached to the substrate.

LARGE SA RESERVES SUGGEST A UNIFYING MECHANISM TO PROTECT MEMBRANE INTEGRITY

To prevent membrane rupture during diverse cellular processes, cells need to keep plasma membrane tension below the lytic level. The two mechanisms often considered in this context are insertion of endomembranes, e.g., via tension-dependent exocytosis (Raucher & Sheetz, 1999; Morris & Homann, 2001), and compensatory V adjustment (Morris & Homann, 2001). Other components of mechanoprotection may include off-loading tension from the bilayer to the subcortical membrane skeleton and maintenance of a highly curved bilayer (discussed in Morris & Homann, 2001; Morris, Wang & Markin, 2003).

Tension-driven SA regulation was first proposed for plant cells, which reversibly internalize membranes to maintain cell integrity (Dowgert, Wolfe & Steponkus, 1987; Shope, DeWald & Mott, 2003).

Similarly, animal cells are also believed to rely on vesicle recruitment to accommodate stretch and cell V changes (Hamill & Martinac, 2001). For example, neurons continuously shuttle membranes between the endomembrane system and the plasma membrane to adjust SA and V, and membrane tension could be a principal feedback mechanism in this process (Morris & Homann, 2001). During hyperosmotic challenge, shrinking neurons are also found to form vacuole-like dilations, membrane invaginations at the substrate-adherent cell surface. Such a process allows neuronal cells to regulate volume, SA and shape, while preserving cell-cell contacts critical for their function. Although insertion of new membranes may be an important mechanism to avoid elevated bilayer tension in neurons, our study with epithelial cells and fibroblasts demonstrates the existence of large SA reserves that are already present on the cell surface, and we provide evidence that these reserves are the main source of the SA increase during moderate (≤ 2 -fold) V expansion. Endomembrane insertion, however, dominates SA adjustment during extreme stresses, and this process may have a tension-dependent component. The use of cell surface reserves by reversible unfolding of excess plasma membrane likely also requires some lower-level membrane tension and, therefore, could be considered another component of tension-dependent SA regulation.

Another mechanism often suggested for keeping plasma membrane tension sublytic is to pump and leak osmolytes (Morris & Homann, 2001). Our study of the kinetics of cell swelling contradicted this view. We found that in response to acute 50% hypotonic shock cells swelled passively to the limits dictated by the imposed osmotic gradient, i.e., about 2-fold V increase, typically within 1.5–3 min (Boudreault & Grygorczyk, 2004a, 2004b) (Fig. 6A). RVD is a much slower process that is initiated only after the cell is already maximally swollen and often after a short delay, resulting in a V plateau, at 3–5 min. RVD is fully completed in about 15 min in A549 cells but requires more than 30 min in NIH 3T3 fibroblasts (Boudreault & Grygorczyk, 2004a). Thus, the RVD process is too slow to counteract acute V increases, and cells need a different mechanism to avoid membrane rupture. Our study suggests that such a mechanism involves, in addition to extensive shape changes, the use of a large excess plasma membrane. The subsequent compensatory transport of osmolytes during RVD is an independent and much slower process with a primary goal of restoring optimal intracellular concentrations of enzymes and metabolites. In this context, resetting the cell's V back to its initial level might be simply a consequence of regulatory adjustment of the intracellular environment rather than the goal in itself. Interestingly, our data also showed that after initial swelling in 50% hypotonic solution both cell V and SA returned close

to their initial levels but their regulatory processes, i.e., the RVD and regulatory surface decrease (RSD) were not directly linked. This was exemplified by the fact that in A549 cells V returned close to its initial level in 10–15 min, while SA remained significantly elevated, even after 20 min (Fig. 6A). Because volume adjustments of irregularly shaped cells might be accomplished, in part, by shape changes without corresponding SA alterations, this results in dissociation of V and SA changes. It also indicates that membrane unfolding is a reversible process but restoration of SA is slower than RVD. A similar observation was made in our previous study (Boudreault & Grygorczyk, 2004a, 2004b). Thus, our data support the view that RVD and RSD are two independent cellular processes, as proposed previously by Morris & Homann (2001). Our observation that both RVD and RSD are blocked by NEM or low temperature (Fig. 6) suggests that these processes require some degree of intracellular trafficking and structural change of the cytoskeleton. Moreover, we reported previously that reducing temperature to 10°C completely abolished the intracellular Ca^{2+} response to hypotonic shock, which may also affect RVD and RSD processes (Boudreault & Grygorczyk, 2004a).

The unexpected finding in our study that all four cell types examined showed huge membrane reserves ($\Delta\text{SA} \approx 280\%$), which included large excess membrane present on the cell surface (60–90% in A549 cells), sheds new light on how cells maintain membrane integrity during rapid V expansion. We propose that such large SA reserves may provide a unifying explanation for the ability of animal cells to sustain sudden mechanical perturbations and to accommodate extensive morphological changes. Large SA reserves may also account for the difficulty in activating mechanosensitive channels in animal cells by buffering membrane tension fluctuations. As a result, in many physiological situations, membrane tension is unlikely to reach levels required to activate such channels, except in special circumstances, such as localized prestressed bilayer regions that may act as a hypothetical mechanosensor (Hamill & Martinac, 2001) or at the cell base of substrate-attached cells (Cemerikic & Sackin, 1993). However, in the latter *in vitro* study, membrane attachment to a rigid glass substrate may be an essential factor responsible for swelling-induced deformation of the cytoskeleton or changes in membrane tension leading to activation of whole-cell currents. Whether this could be reproduced on a flexible substrate, more resembling the *in vivo* situation, needs future experimental verification. Large SA reserves were also found in osmosensory neurons (Zhang & Bourque, 2003), but contrary to our notion, it was concluded that this would allow mechanogated channels to sense tension changes during cell V expansion or contraction. The conclusion was based on the assumption that, in

neurons, membrane tension is transmitted indirectly to the channel, via the membrane-associated cytoskeleton, consistent with a “tethered” model of channel gating. Such a mechanism, however, is still debated and, unlike the “bilayer” model, lacks unequivocal experimental support (Hamill & Martinac, 2001).

It should be underlined that our conclusion on the major impact of intracellular membrane reserves on the osmotic resistance of nucleated cells is consistent with studies of mammalian erythrocytes. In these highly specialized cells lacking intracellular membrane reserves, plasma membrane rupture occurs under modest (~70%) V increase and is accompanied by discocyte-spherocyte shape transition (Kageyama et al., 1989).

In summary, the presence of large SA reserves in all four mammalian cell lines examined in this study suggests that this is not an exception but might be a common feature of many cell types. In particular, the sizable fraction of reserves present on the cell surface as excess plasma membrane may provide a simple mechanism to maintain membrane tension below the lytic level during various cellular processes or acute mechanical perturbations.

This study was supported by the Canadian Institutes of Health Research, the Canadian Cystic Fibrosis Foundation and Natural Sciences and Engineering Research Council of Canada. We thank Dr. Jean-Yves Lapointe for help during the development of our imaging technique; Drs. Cathy Morris, Fred Sachs and Andrzej Kubalski for their comments on the manuscript; and Ms. Helene Chabot for technical assistance.

References

- Boudreault, F., Grygorczyk, R. 2004a. Cell swelling-induced ATP release is tightly dependent on intracellular calcium elevations. *J. Physiol.* **561**:499–513
- Boudreault, F., Grygorczyk, R. 2004b. Evaluation of rapid volume changes of substrate-adherent cells by conventional microscopy 3D imaging. *J. Microsc.* **215**:302–312
- Cemerikic, D., Sackin, H. 1993. Substrate activation of mechanosensitive, whole cell currents in renal proximal tubule. *Am. J. Physiol.* **264**:F697–F714
- Cozens, A.L., Yezzi, M.J., Kunzelmann, K., Ohri, T., Chin, L., Eng, K., Finkbeiner, W.E., Widdicombe, J.H., Gruenert, D.C. 1994. CFTR expression and chloride secretion in polarized immortal human bronchial epithelial cells. *Am. J. Respir. Cell Mol. Biol.* **10**:38–47
- Dowgert, M.F., Wolfe, J., Steponkus, P.L. 1987. The mechanics of injury to isolated protoplasts following osmotic contraction and expansion. *Plant Physiol.* **83**:1001–1007
- Gilbert, H.F. 1990. Molecular and cellular aspects of thiol-disulfide exchange. *Adv. Enzymol. Relat. Areas Mol. Biol.* **63**:69–172
- Graf, J., Rupnik, M., Zupancic, G., Zorec, R. 1995. Osmotic swelling of hepatocytes increases membrane conductance but not membrane capacitance. *Biophys. J.* **68**:1359–1363
- Hamill, O.P., Martinac, B. 2001. Molecular basis of mechanotransduction in living cells. *Physiol. Rev.* **81**:685–740
- Ingber, D.E. 2003. Tensegrity I. Cell structure and hierarchical systems biology. *J. Cell Sci.* **116**:1157–1173
- Jackson, R.C., Modern, P.A. 1990. *N*-Ethylmaleimide-sensitive protein(s) involved in cortical exocytosis in the sea urchin egg: localization to both cortical vesicles and plasma membrane. *J. Cell Sci.* **96**(Pt 2):313–321
- Jewell, S.A., Bellomo, G., Thor, H., Orrenius, S., Smith, M. 1982. Bleb formation in hepatocytes during drug metabolism is caused by disturbances in thiol and calcium ion homeostasis. *Science* **217**:1257–1259
- Kageyama, K., Onoyama, Y., Kogawa, H., Goto, E., Tanabe, K. 1989. The maximum and minimum water content and cell volume of human erythrocytes in vitro. *Biophys. Chem.* **34**:79–82
- Karlsson, R., Lindberg, U. 1985. Changes in the organization of actin and myosin in non-muscle cells induced by *N*-ethylmaleimide. *Exp. Cell Res.* **157**:95–115
- Lemasters, J.J., DiGiuseppi, J., Nieminen, A.L., Herman, B. 1987. Blebbing, free Ca^{2+} and mitochondrial membrane potential preceding cell death in hepatocytes. *Nature* **325**:78–81
- McManus, M.L., Churchwell, K.B., Strange, K. 1995. Regulation of cell volume in health and disease. *N. Engl. J. Med.* **333**:1260–1266
- Mongin, A.A., Orlov, S.N. 2001. Mechanism of cell volume regulation and possible nature of the cell volume sensor. *Pathophysiology* **8**:77–88
- Morris, C.E., Homann, U. 2001. Cell surface area regulation and membrane tension. *J. Membr. Biol.* **179**:79–102
- Morris, C.E., Wang, J.A., Markin, V.S. 2003. The invagination of excess surface area by shrinking neurons. *Biophys. J.* **85**:223–235
- Nakamura, F., Pudas, R., Heikkinen, O., Permi, P., Kilpelainen, I., Munday, A.D., Hartwig, J.H., Stossel, T.P., Ylanne, J. 2006. The structure of the GPIb-filamin A complex. *Blood* **107**:1925–1932
- Nichol, J.A., Hutter, O.F. 1996. Tensile strength and dilatational elasticity of giant sarcolemmal vesicles shed from rabbit muscle. *J. Physiol.* **493**(Pt 1):187–198
- Olson, J.E., Li, G.Z. 1997. Increased potassium, chloride, and taurine conductances in astrocytes during hypoosmotic swelling. *Glia* **20**:254–261
- Raucher, D., Sheetz, M.P. 1999. Characteristics of a membrane reservoir buffering membrane tension. *Biophys. J.* **77**:1992–2002
- Renstrom, E., Eliasson, L., Bokvist, K., Rorsman, P. 1996. Cooling inhibits exocytosis in single mouse pancreatic B-cells by suppression of granule mobilization. *J. Physiol.* **494**(Pt 1):41–52
- Ross, P.E., Garber, S.S., Cahalan, M.D. 1994. Membrane chloride conductance and capacitance in Jurkat T lymphocytes during osmotic swelling. *Biophys. J.* **66**:169–178
- Shope, J.C., DeWald, D.B., Mott, K.A. 2003. Changes in surface area of intact guard cells are correlated with membrane internalization. *Plant Physiol.* **133**:1314–1321
- Strange, K. 2004. Cellular volume homeostasis. *Adv. Physiol. Educ.* **28**:155–159
- Wan, X., Harris, J.A., Morris, C.E. 1995. Responses of neurons to extreme osmomechanical stress. *J. Membr. Biol.* **145**:21–31
- Zhang, Y., Hamill, O.P. 2000. On the discrepancy between whole-cell and membrane patch mechanosensitivity in *Xenopus* oocytes. *J. Physiol.* **523**(Pt 1):101–115
- Zhang, Z., Bourque, C.W. 2003. Osmometry in osmosensory neurons. *Nat. Neurosci.* **6**:1021–1022